Li-ion cell safety monitoring using mechanical parameters, Part II: battery behavior during thermal abuse tests

Angel Kirchev, Nicolas Guillet, Loic Lonardoni, Sebastien Dumenil, Vincent Gau

Li-ion cell safety monitoring using mechanical parameters, Part 2: battery behavior during thermal abuse tests

A. Kirchev*, N. Guillet, L. Lonardoni, S. Dumenil, V. Gau

Univ. Grenoble Alpes, CEA, Liten, Campus Ines, 73375 Le Bourget du Lac, France

*corresponding author e-mail: angel.kirchev@cea.fr

Key words: lithium ion battery, thermal safety, strain gauge, ultrasound interrogation, external short-circuit

Research highlights:

- Extended monitoring of Li-ion battery operation during thermal abuse tests
- The ultrasound interrogation provides early alert for slowly approaching overheating
- The battery deformation measurement accounts very rapidly short-circuit events
- The decrease of the state of charge increases markedly the battery safety

Abstract

Acoustic ultrasound interrogation and deformation measurements have been used simultaneously as supplementary battery monitoring methods during external overheating and external short-circuit safety tests of LG INR-18650 MJ1 (NMC 811- G-SiO_x) Li-ion cells. The short-circuit experiments showed that the MJ1 technology is protected against this type of thermal abuse by the current interruption device (CID) integrated in the positive terminal of the cell. The results indicate that the strain gage signal is able to provide very rapid alert for this type of battery safety breach due to an abrupt change of the cell pressure. It precedes the time of the increase of the skin temperature by an order of magnitude. The thermal stability experiments carried out in adiabatic rate calorimeter on completely charged and overcharged batteries at open circuit conditions, showed that the MJ1 technology is susceptible to self-heating by slow internal exothermic reactions starting above 60 °C. The subsequent process of thermal runaway starts when the temperature exceeds 140 C. The results from the extended monitoring of the cells during the thermal stability tests showed that the acoustic ultrasound interrogation data combined with data mapping and clustering of the signal provides advantageous indication for early detection of slowly approaching battery safety breach events.

1. Introduction

The lithium-ion battery safety testing can be carried out at conditions representing different mechanical, thermal and electric abuse events happening under various circumstances. The mechanic abuse tests such as nail penetration or cell crushing, aim causing cell deformations similar to those happening during a car crash. Such kind of events cause an internal short-circuit producing locally large amount of heat which may cause further appearance of battery fire or even an explosion. On the other hand, the thermal abuse events take place when the cell temperature exceeds the safety maximum provided by the manufacturer. This can be caused by the cell exposure to high temperature from external source including a short-circuited neighbor cell, or a self-heating resulting from a combination of Joule effect and poor heat exchange [1 - 3]. The increase of the cell temperature above certain point, which is different for each different Li-ion battery technology, triggers the start of exothermic chemical reactions. According to the literature, the latter proceeds between the electrolyte solvent and the lithiated graphite or carbon particles via decomposition of the corresponding solid-electrolyte interface (SEI) [4]. If the cell temperature continues increasing further, other more exothermic reactions such as negative electrodes decomposition, electrolyte decomposition and oxygen release from metallic oxides crystalline structures of the positive electrode [5, 6]. At certain point the temperature rate starts rising very rapidly marking the start of the thermal runaway [7]. Alternatively, the thermal runaway can be triggered by the chemical and electrochemical reactions taking place during the overcharge of the cell or by the application of external short circuit [1,2]. The early detection of the above-mentioned battery safety breach events is a task of critical importance for each battery monitoring and management system (BMS). The aim of this work is a study of the mechanical behavior of 18650 lithium-ion batteries during thermal abuse experiments caused by external overheating and external electric short-circuit discharge using strain gage and acoustic ultrasound interrogation measurements, which may serve as additional safety indicators.

2. Experiment and methods

The experiments have been carried out on lithium-ion cells from type INR18650 MJ1 (denoted as MJ1) manufactured by LG Chem (Republic of Korea). The rated voltage and capacity of the cells are 3.7 V and 3400 mAh. The cells have been instrumented with rectangular rosette stain gauges “C2A-06-062LR-120” (Micro-Measurements, USA), a pair of piezoelectric transducers EPZ-20MS64W (6.4 kHz, 400 ohms) and K-type thermocouple. The thermal abuse experiments have been performed in adiabatic Accelerating Rate Calorimeter (ARC) manufactured by the US company Thermal Hazard Technology. The other experimental set-up details can be found in first part of this publication series [8].

3. Results and discussion

3.1. External short-circuit tests at constant resistance

The external short-circuit of a battery can be considered as a discharge process carried out at very high current density (or at high discharge rate) using a resistor. This experiment has been set up in a blast box at room temperature. Two different series of tests have been performed. During the first one, cells

with different state of charge (SOC) have been short-circuit discharged using a resistor with a fixed resistance rating. Figure 1 presents the evolution of the battery parameters monitored during the short-circuit experiments using a constant shunt resistance equal to 40 mOhm. The latter is slightly higher than the internal resistance of the cell which is about 30 mOhm at SOC = 50 % and room temperature [8]. Four characteristic values of SOC have been selected: 0, 50, 100 and 115 %. The latest has been achieved by a constant current / constant voltage overcharge starting with C/2h-rated current and limited by a floating charge with 4.6 V during 6 hours (C denotes the nominal capacity of the cell). The short circuit current has been monitored by a current transducer manufactured by LEM SA (Switzerland) linked to an electrochemical test bench Biologic (France). The short circuit test was started by a switching device connecting the cell with the resistor used for the high-rate discharge controlled by the Biologic test bench.

Figure 1a shows that the peak of the discharge current observed during the short circuit test corresponds to the cell with the highest SOC, *i.e.* to the overcharged cell. It decreases with the decrease of the state of charge. In the same time, the duration of the short-circuit discharge increases at the cells with lower initial SOC. The cell voltage evolution remains rather similar (Figure 1b), being comprised of initial voltage drop related to the high discharge current, followed by a voltage arrest and next voltage drop to zero. The discharge current has been integrated and the resulting evolution of SOC is shown in Figure 1c. It can be seen that the short-circuit discharge expends only a fraction of the cell capacity (10 – 20 % depending on the initial SOC) before the voltage drops to a zero level. In order to analyze further the mechanism of the short-circuit discharge process, the cell voltage has been plotted against the current (Figure 1d). The obtained plots show clearly a linear relationship between current and voltage with approximately the same slope and intercept for all four tested cells. The linear fit results show a resistance of 42 mOhm and intercept close to zero. Figure 1e presents the evolution of the cell skin temperature during the short-circuit discharge. The temperature increases very rapidly in the case of fully charged or overcharged cells (about 75 °C/min during the first 30 s of the short-circuit discharge). The discharge of the overcharged cell is terminated by the activation of the current interruption device (CID) after 40 s, while the temperature reaches a maximum of 84.5 °C after 53 s. In the case of the cell with initial SOC equal to 100 %, the discharge lasts 64 s allowing a temperature rise to 117.9 °C after 84 s since the beginning of the short-circuit.

The increase of the temperature during the short-circuit of the cell with SOC = 50 % is much less intense due to the lower discharge current despite the longer discharge time. However, it should be noted that even at zero SOC the cell remains a source of electric power able to generate a current in the range of 10 A for several tens of seconds.

The thermal behavior of the cells during the short circuit can be first-order analyzed using the following approach. The temperature increase can be expressed thermodynamically as:

$$\Delta T = \frac{Q_{irrev}}{mC_p} \qquad (1)$$

where Q_{irrev} is the heat energy dissipated by the cell during the short-circuit (J), C_p is the heat capacity of the cell ($J.K^{-1}.g^{-1}$), and m the mass of the battery. From the other hand, Q_{irrev} can be considered as Joule heat:

$$Q_{irrev} = R_{int} I_{av}^2 t \qquad (2)$$

where R_{int} is the internal resistance of the cell (Ohm), I_{av} is the discharge average current (A), and t is the duration of the short circuit (s). In this way, the temperature increase during the short circuit test can be expressed as:

$$\Delta T = \frac{R_{int} I_{av}^2 t}{m C_p} \qquad (3)$$

Figure 1f presents the plot of the ΔT considered as the difference between the maximum and the initial temperature vs. the product "$I_{av}^2 t$". The point corresponding to $\Delta T = 0$ / $I_{av} = 0$ has been added in order to represent the thermal behavior of the cells during OCV prior to the short-circuit. According to the last equation, the data in Figure 1f should be fitted with linear regression. The fitting results show good correlation with a straight line ($R^2 = 0.968$), an interception of 0.3 °C (*i.e.* fairly close to the expected value of 0 °C), and a slope equal to 6.21 x 10^{-4} °C A^{-2} s^{-1}. It has been seen that the current / voltage behavior of the cell during the short-circuit is rather limited by the resistance of the external circuit, which on its term is higher than the "nominal" value of the internal resistance of the cell. If we use the latter (31 mOhm @ SOC = 50 % and 1 kHz) in order to calculate the heat capacity, the result is 49.9 $J.K^{-1}$ or 1.08 $J.g^{-1}.K^{-1}$ considering a nominal weight of the cell equal to 46.3 g. This result is in good agreement with the measurement of C_p of 18560 Li-ion cells estimated by adiabatic calorimetry, the latter being in the range of 0.98 – 1.04 $J.g^{-1}.K^{-1}$ [9].

Figure 1g presents the evolution of the deformation of the cell in direction of the jellyroll circumference (*i.e.* the strain signal "J2"). It can be seen that almost immediately after the application of the short-circuit discharge, there is a rapid swelling of the cell which passes through a maximum and decreases further. If we compare this behavior with the results corresponding to regular discharge discussed in the previous paper [6], it is evident the initial swelling is due to undesirable processes, since the regular discharge causes a retraction of the cell diameter.

Figure 1h presents the evolution of the received acoustic signal strength during the short circuit test. It can be seen that the application of high rate discharge causes rapid drop of the signal strength corresponding to increasing absorption of ultrasound. After the termination of the short-circuit discharge, the signal strength starts increasing, as long as the cell SOC remains higher than zero. The acoustic data have been analyzed further using data clustering and mapping of the power spectral density (PSD) of each ultrasound interrogation point. The results presented in the supplementary information (S1) shows the main changes in the physical properties of the acoustic signal can be correlated with the decrease of the cell voltage (and SOC) and the increase of the temperature with time.

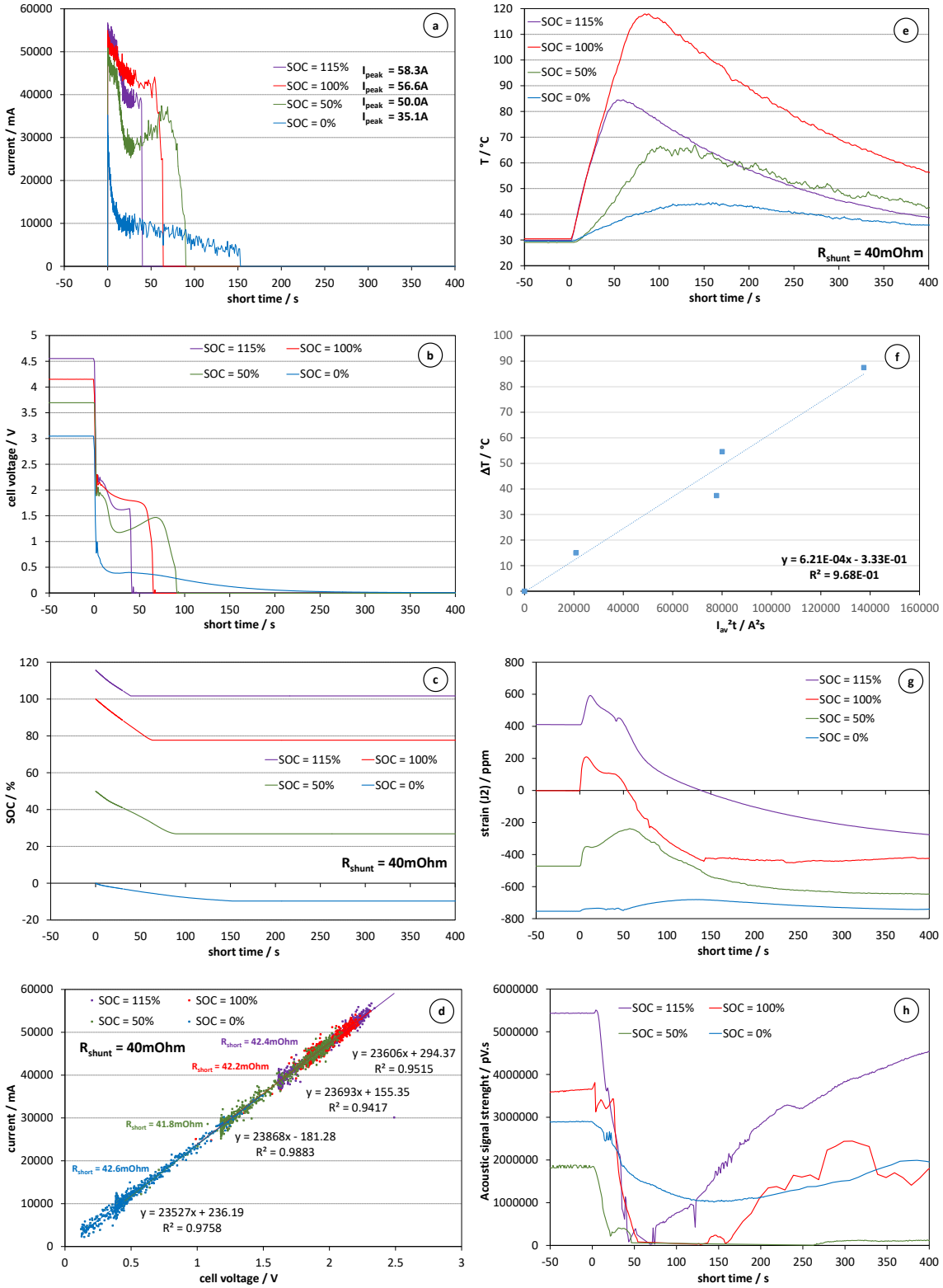

Fig. 1. Evolution of the discharge current (a), cell voltage (b), SOC (c), skin temperature (e), strain (g) and acoustic signal strength (h) during short circuit experiments with 40 mOhm rated shunt. Volt-Ampere characteristics of the cells during the short-circuit tests (d). Analysis of the thermal behavior of the cells during the short-circuit (f).

The mechanism of the undesirable very rapid swelling process can be attributed to the increasing temperature and/or formation of gases, which increase the pressure in the cell. The retraction of the cells coincides roughly with the cooling down of the cell skin temperature. The correlation between the strain and SOC remains rather qualitative, probably due to irreversible changes inside the cells due to the extremely high rate of the discharge. The mechanism of the cell casing deformation during the short circuit tests has been further evaluated by the parametric analysis [10] presented briefly in the supplementary information (**S2**). It is also discussed in more details in the Part 1 of this series [8]. The corresponding results are shown in Figure 2. The point of reference of axis (r=0, D= 0) has been chosen to correspond to the deformation of completely charged 18650 cell. The data points are separated in three domains corresponding to the initial increase of the temperature up to 70 °C, the further increase of the temperature until reaching a maximum, and a last period of cool down. It can be seen that the mechanism of the cell deformation during the short-circuit discharge depends strongly on the initial SOC value. In the case of overcharged cell the deformation due to the short-circuit discharge follows a pattern of initial cylindrical expansion (Ex) followed by a spherical retraction (Rt) and further close-to-isotropic shrinkage (Sh) due to the temperature cool down. When the initial SOC of the cell is equal to 100 %, the cell deformation starts as a cylindrical expansion (Ex), which continues as torsion (T) with the progression of the heating. During the subsequent cooling, the deformation follows a pattern corresponding to compression(C). The pattern of r(D) function during the short-circuit test of the cell with initial SOC = 50 % starts also with cylindrical expansion followed by torsion and isotropic shrinkage during the cooling. The deformations during the testing of the completely discharged cell are the smallest, which can be related to the small change of SOC and the small increase of the temperature. The presence of the torsion sections in the r(D) plots in Figure 2b and 2c can be related to the appearance of pressure gradients attempting to unwind the cell jellyroll.

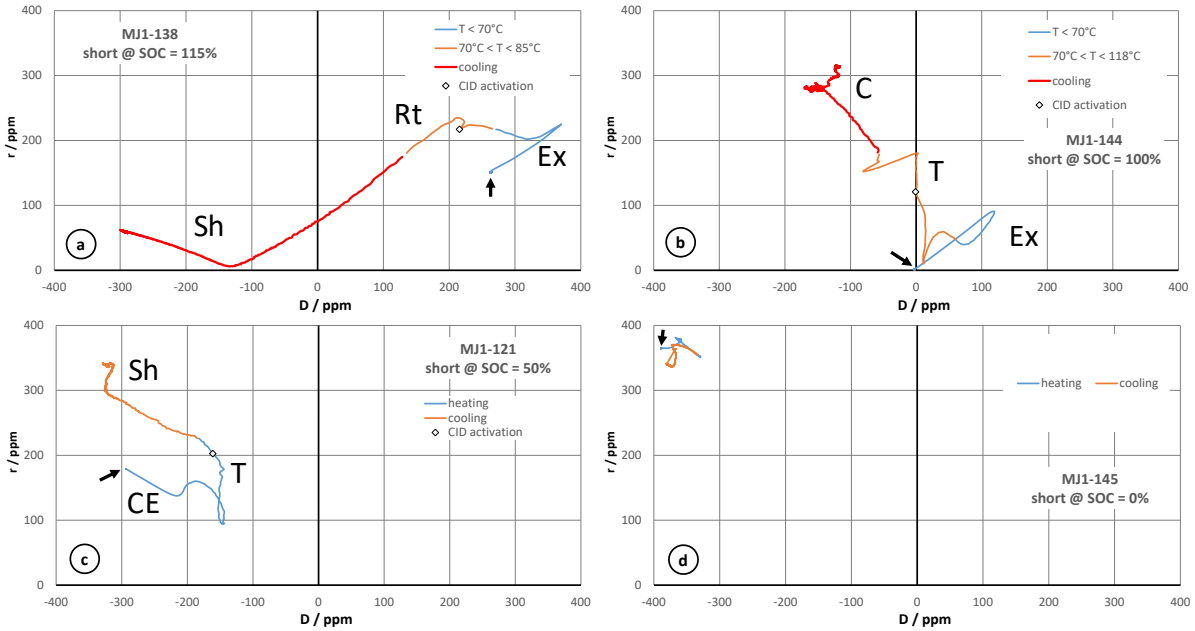

Fig. 2. Parametric analysis of the cell strain behavior during the short-circuit tests of MJ1 cells at different SOC using a shunt resistance equal to 40 mOhm. The starting point of the experiment is marked with black arrow.

3.2. External short-circuit tests at constant SOC

The second series of experiments has been carried out on completely charged cells (SOC = 100 %) using four different shunts with rated resistance of 2, 10, 20 and 40 mOhm. In this way different peaks of the short-circuit current have been applied on the MJ1 cells. The results from this experiment are summarized in Figure 3. It can be seen that the discharge current and duration as well as the cell voltage (Figure 3a and Figure 3b) correlate very well with the rated resistance of the shunt: the highest discharge current is measured during the short-circuit test using 2 mOhm shunt (about 35C-rated discharge). During this test, the cell voltage is lowest (about 0.1 V) and it is terminated by the activation of the CID after less than one second. The discharge current decreases when the used shunt resistance is higher, while the voltage plateau and the discharge duration both increased. The integration of the discharge current and the calculation of SOC presented in Figure 3c shows that the short-circuit discharge expends relatively small fraction of the discharge capacity before the activation of the CID by the rapid increase of the internal temperature and pressure. The quantitative analysis of the current vs. voltage data shown in Figure 3d indicates an ohmic behavior with a resistance (R_{short}) values matching fairly close the rated shunt resistances. The latter is in good agreement with the results presented in Figure 1d.

The evolution of the temperature on the surface of the MJ1 cells during the short-circuit tests with various resistors is shown in Figure 3e. It can be seen that the resistance of the short circuit exerts very strong effect on the thermal behavior of the cell. In the case of short-circuit with very low resistance (*e.g.* 2 mOhm), the increase of the internal temperature and pressure are almost immediate, resulting in rapid activation of the CID and almost negligible increase of the skin temperature of the cell. In the case of the short-circuit tests with 10 and 20 mOhm shunts, the initial increase of the temperature is almost identical which can be related to the similar profile of the current. Again, the maximum temperature is reached with a delay of about 20 s after the discharge termination. The data show that there is a critical resistance of the short-circuit corresponding to a maximum of the temperature which can be attained. Under the applied experimental conditions (single cell at room temperature with passive air cooling) the critical resistance is close to 20 mOhm. The temperature maximum achieved in the last case is 129 °C, which is below the runaway temperature of 140 °C measured in adiabatic conditions (using ARC), and discussed in the next paragraph. The thermal behavior of the cell has been also analyzed using the above-mentioned first-order approach (Fig. 3f). The results from linear fit indicate a heat capacity of the cell equal to 1.04 $J.g^{-1}.K^{-1}$, which is even closer to the results from the literature [9].

The evolution of the strain of the cell casing diameter presented in Figure 3g confirms that this parameter is very sensitive against a short circuit abuse with a reaction time of 1 – 5 seconds, which precedes the increase of the temperature several times (the temperature maximums are attained after 20 – 40 s). The considerable delay between the cell swelling and the cell skin heating suggests that the rapid initial deformation detected by the strain gage is due to the build-up of gas pressure. It should be noted also that the transients of the strain during the short-circuit tests with varying shunt resistance remain similar to those presented in Figure 1g.

The evolution of the strength of the received ultrasound acoustic signal during the short-circuit tests with varying shunt resistance is presented in Figure 3h. The change of the signal strength in the case of 2 mOhm-rated shunt is very small which can be explained with the negligible change of the cell temperature and SOC prior to the activation of the CID. For the rest of the cases, the high-rate discharge and the increased temperature cause significant decrease of the signal strength running together with the short-circuit indicating increased absorption of the ultrasound.

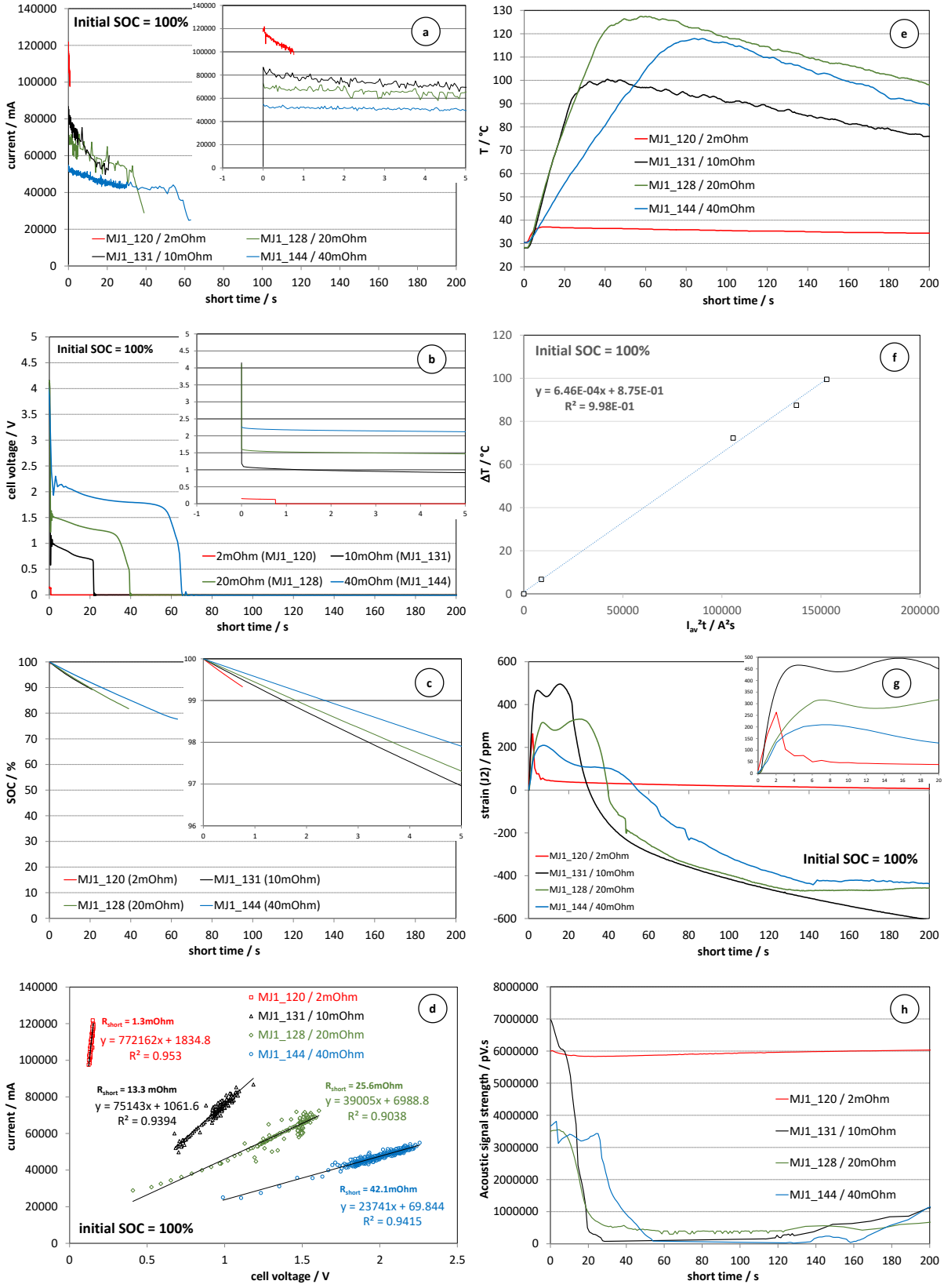

Fig. 3. Evolution of the discharge current (a), cell voltage (b), SOC (c), skin temperature (e), strain (g) and acoustic signal strength (h) during short circuit tests of completely charged MJ1 cells using shunts with different resistance. Volt-Ampere characteristics of the cells during the short-circuit tests (d). Analysis of the thermal behavior of the cells during the short-circuit (f).

Figure 4 presents the parametric analysis of the cell strain data acquired during the short-circuit tests with rated shunt resistance equal to 2, 10 and 20 mOhm. The short-circuit carried out with the smallest resistance, which has been terminated most rapidly is associated with the smallest deformation corresponding to an isotropic expansion followed by a retraction back to the initial point. This result correlates well with the observed small changes of the SOC and the temperature. It indicates that the deformation is caused by nearly instantaneous buildup of gas pressure inside the cell. The high-rate discharge using the other two shunts starts also with an isotropic expansion, however it proceeds differently depending on the used resistance. In the case of short-circuit with 10 mOhm shunt, the deformation mechanism starts as isotropic expansion followed by a compression which evolves into isotropic shrinkage during the cool down of the cell. It must be denoted that shortly after the start of the shrinkage process, the discharge is terminated by the activation of the CID, indicating that the beyond this point the deformation is related to relaxation processes and heat dissipation. The short-circuit through a shunt with 20 mOhm rated resistance, which causes the highest increase of the temperature, is associated with the appearance of torsion effects similar to those observed during the high-rate discharge with 40 mOhm rated shunt (Figure 2d).

It can be concluded that the observed complex deformation mechanism can be related to several phenomena with antagonistic mechanical effects: from one hand the increasing temperature and the associated generation of gaseous products are causing the initial expansion, from the other, the discharge process and the subsequent mechanical relaxation are associated with shrinkage of the cell roll diameter. It can be supposed too, that there is a non-homogeneous spatial distribution of the formation of gaseous products inflicting the observed torsion effects due to the appearance of mechanic force trying to unwind the cell jellyroll.

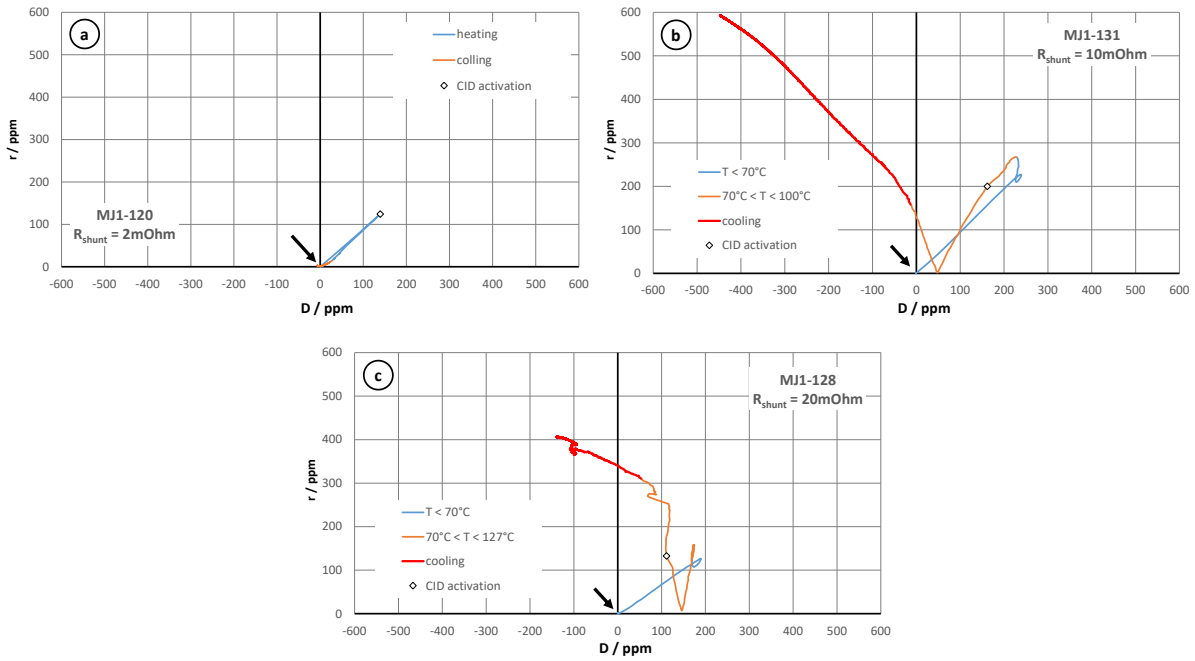

Fig. 4. Parametric analysis of the cell strain behavior during the short-circuit tests of MJ1 cells at SOC = 100 % using shunts with rated resistance equal to 2, 10 and 20 mOhm. The starting point of the experiment is marked with black arrow.

The short-circuit tests show that the increase of the internal pressure is much faster than the increase of the temperature. The evaluation of the impact of this parameter on the cell casing deformation and the operation of the CID has been carried out using a modified test set-up for pressure transducers calibration presented in the supplementary information (S3). The test has been carried out on MJ cell casing with cut bottom terminal and removed cell jellyroll. This cell casing has been equipped with a sealing brass ring and a strain gage mounted in the middle of the distance between the positive terminal and the edge of the brass ring using the same rosette orientation (the gage J2 accounts the change of the cell diameter). The positive cell terminal and the side wall of the cell have been short circuited from the inside using a spring-like stainless steel wire. Thus prepared, the cell casing has been mounted in the set-up allowing slow manual increase of the pressure using deionized water as a working fluid. In order to estimate the pressure corresponding to the activation of the CID, a constant current of 10 mA has been applied between the positive terminal and the cell wall and the resulting voltage has been monitored together with the strain.

Figure 5a and 5b present the evolution of the cell casing strain, the hydrostatic pressure and the ohmic drop across the positive terminal during this experiment carried out at 23 °C. The results indicate that there is an excellent correlation and synchronism between the evolution of the pressure and the readings of the strain gage. The readings of the middle gage (J2) are markedly higher than those of J1 and J3, indicating a preferential increase of the cell casing diameter and smaller deformation of the cell casing length.

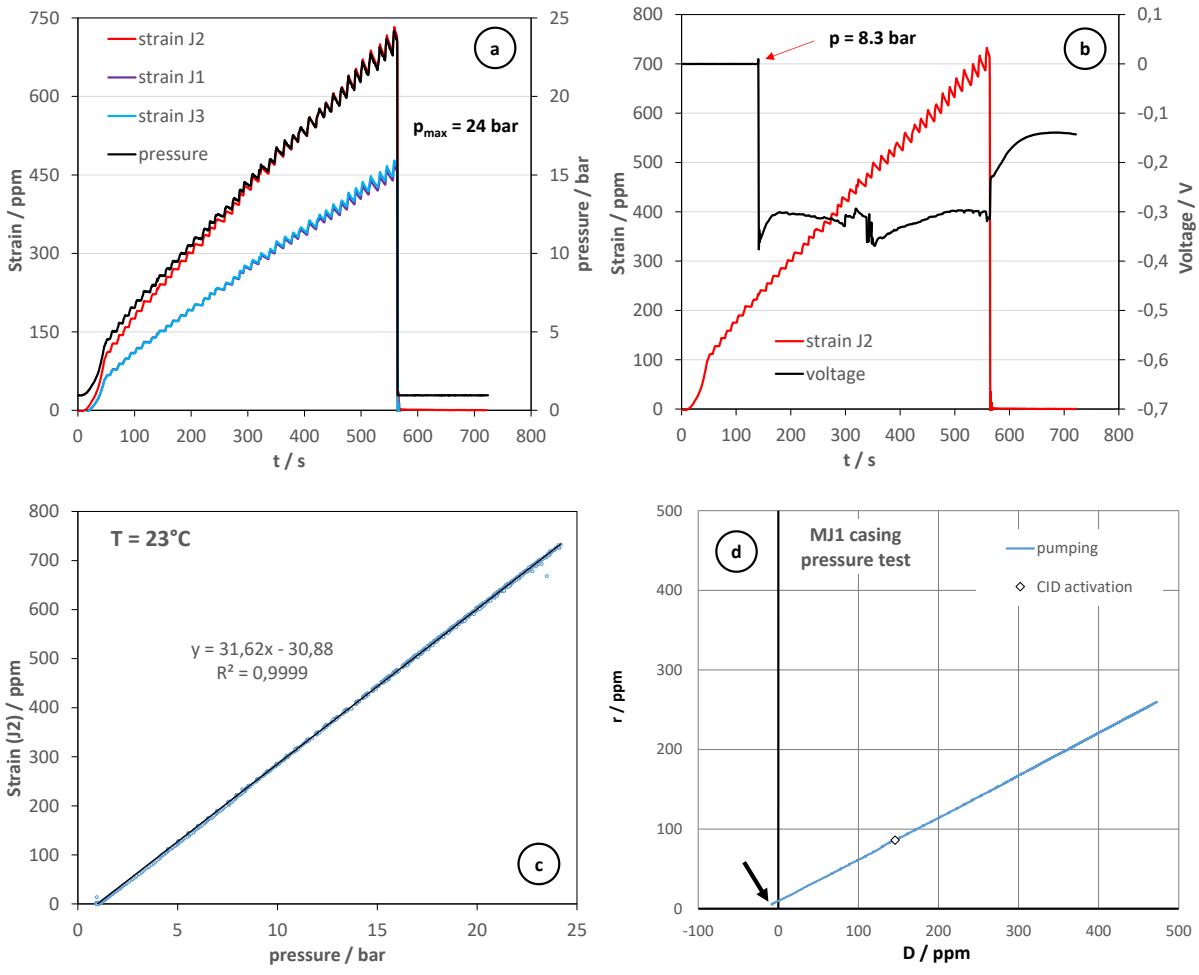

Fig. 5. Impact of the hydrostatic pressure on the cell casing deformation and the CID operation.

The pressure increased to 24 bar and then it dropped abruptly due to opening of the cell safety valve, which has been visualized by the sudden appearance of water spill from the positive terminal. This event coincided with a sudden drop of the strain. Both, the pressure and the strain returned to their initial values indicating that the observed deformation was completely elastic. The latter has been confirmed further by the linear relationship between the hydrostatic pressure and the readings of the strain showed in Figure 5c. On the other hand, the comparison between the voltage signal at 10 mA with the cell strain evolution and the hydrostatic pressure, presented in Figure 5 a-c, shows that there is an abrupt voltage drop at pressure equal to 8.3 bar. This event indicates an increase of the positive terminal resistance due to the activation of the current interrupting device integrated in the cell. The estimated values of the pressure of the CID activation and the cell venting are in good agreement with the results of Weisi Li *et al.* obtained for the same Li-ion technology (MJ1) by using a different set-up based on gaseous nitrogen as pressure regulation fluid [11]. The parametric analysis of the deformation pattern due to the internal hydrostatic pressure shown in Figure 5d indicates that the increase of this parameter causes predominant expansion of the cell diameter and rather negligible change of the cell length. The ensemble of the results in Figure 5 confirms the above-mentioned hypothesis that the initial very rapid increase of the strain signals observed at most of the short-circuit tests is due to a very fast build-up of internal pressure due to formation of gaseous phases either by electrolyte solvent boiling or by chemical/electrochemical processes related to the SEI decomposition.

3.3. Thermal abuse tests

The thermal abuse tests have been carried out in adiabatic calorimeter. The first stage of the calorimetric experiments was the calibration of the equipment which has been done using an aluminum alloy (2017A – AU4G) cylinder with a diameter of 18 mm and length of 65 mm (*i.e.* same dimensions as those of MJ1 cell). During the second stage, a completely charged cell MJ1 without any sensors has been subjected to thermal abuse experiment using “heat, wait, seek” sequence during which the cell temperature is increased step-wise by 5 °C increments. After the detection of the first exothermic event, the cell is maintained at adiabatic conditions resulting in further self-heating process, which may evolve into a thermal runaway. Figure 6 presents the evolution of the cell skin temperature with the time (a) and the dependence of the temperature rate on the cell skin temperature (b). The summary of this experiment provided by the ARC software is listed in Figure 6b. The results show that the first exothermic process starts at 60 °C. Above this temperature the heating rate increases progressively up to 118 °C, where a first endothermic process is detected (it can be hypothesized as the beginning of an evaporation process). At 140 °C the cell reaches the runaway temperature. Beyond this point, the rate of the exothermic processes becomes fast enough to heat the battery by itself, rapidly resulting in overheating. The maximum temperature reached during the experiment was 156 °C, after which the cell was cooled down to room temperature using a flush of compressed air. The inspection of the cell geometry after the ARC test showed a leakage of electrolyte without any changes of the cell dimensions. The weight of the cell decreased to 43.6 g from the initial weight of 46.3 g. The open circuit voltage of the cell was zero and the AC internal resistance at 1 kHz was above 3 Ohm. The obtained results explain rather well the thermal behavior of the MJ1 cells during the short-circuit tests, where the early activation of the CID prevented the increase of the cell temperature above 130 °C.

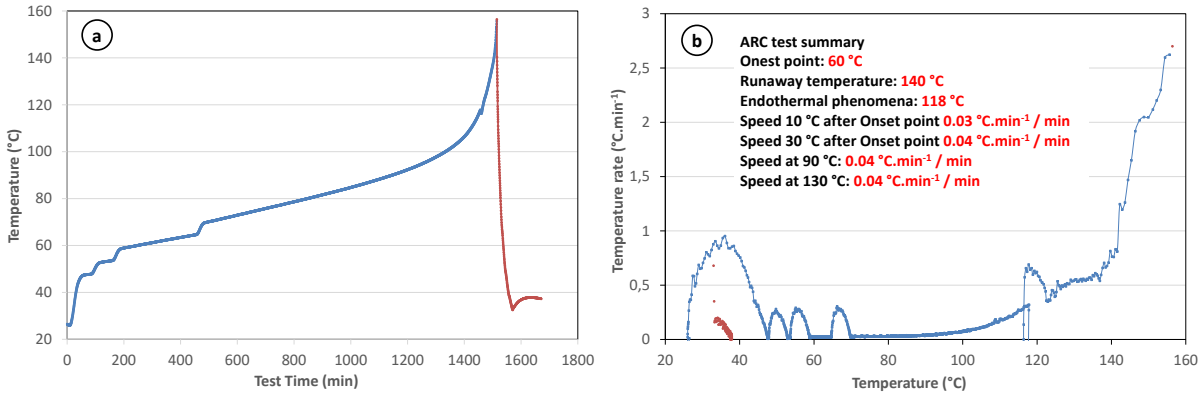

Fig. 6. Evolution of the cell skin temperature with the time (a) and dependence of the temperature rate on the cell skin temperature (b) during thermal abuse test of MJ1 cell in accelerating rate calorimeter (SOC = 100 %).

During the third stage of the thermal abuse tests, four cells equipped with strain gauges and acoustic transducers have been subjected to over-heating in the ARC at different states of charge. The selected SOC points were equal to 0, 50, 100 and 120.3%. In first three cases, the cells have been equipped with spot-welded tabs and wires allowing the monitoring of the cell open circuit voltage during the thermal abuse experiments. In the last case, the cell voltage was not accessible since the overcharge to 120.3% caused activation of the current interruption device.

Figure 7 presents the evolution of the battery parameters monitored during the thermal abuse tests at different SOC. The time scale was reset to zero in the moment when the cell skin temperature exceeded 35 °C in order to facilitate the comparison of the transients. The presence of considerable number of wires connected to the cell, caused a change of the temperature profiles applied by the ARC. Thus instead of the initial step-wise increases of the temperate, the calorimeter increased the temperature quasi-linearly from 30 to 110-130 °C. The comparison of the data plotted in Figure 7 shows that the SOC value is crucial for the safety of the MJ1 cells. In the case of low SOC (0 and 50 %) the cells are heated up to 160 °C and cooled down to room temperature without the apparition of any hazardous phenomena different from the electrolyte venting. In contrary, the completely charged cell and the overcharged cell went in thermal runaway mode, which evolved extremely rapidly into battery fire with peak temperatures exceeding 490 – 560 °C. The evolution of the temperature during the ARC tests shows clearly that the decrease of the SOC increases progressively the battery resistance against thermal abuse. This trend can be seen further in the evolution of the OCV presented in Figure 7b. The increase of the battery temperature caused rather small change of the OCV with a trend depending on SOC, until a moment of instantaneous drop of this parameter. Obviously this event corresponds to the activation of the CID which results in increase of the cell internal resistance with several orders of magnitude. Since the CID activation is caused by a pressure built-up in the cell, it can be supposed that the increase of the temperature activates chemical reactions forming gaseous products. It can be seen that the temperature of the activation of the CID increases with the increase of the depth of discharge from 104 °C for a completely charged cell to 122 °C for a completely discharged cell.

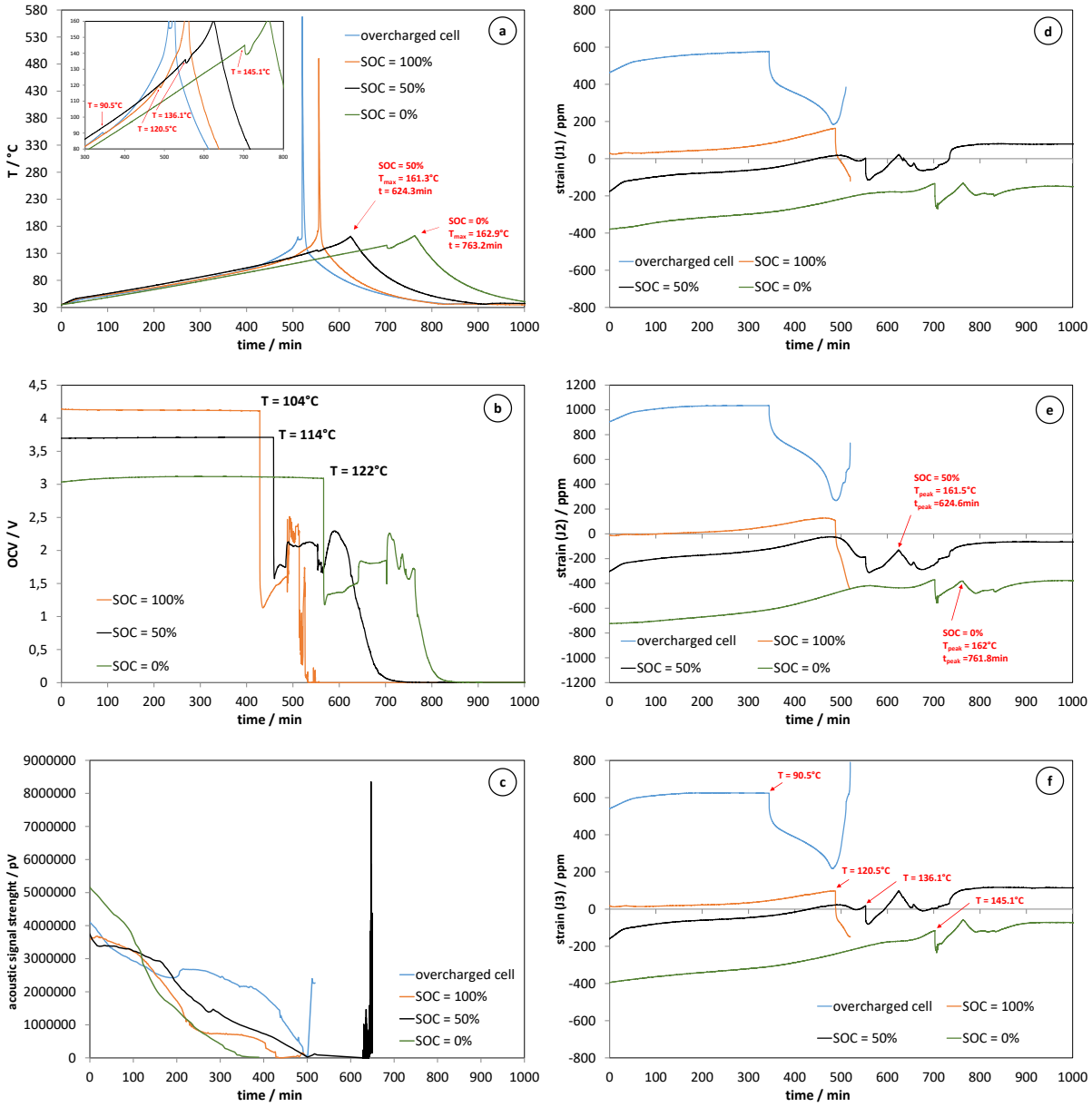

Fig. 7. Evolution of the cell casing temperature (a), voltage (b), received acoustic signal strength (c) and strain (d-f) with the time during thermal abuse tests of MJ1 cells with different state of charge.

The evolution of the cell casing deformation during the thermal abuse tests is presented in Figure 7d-f. It can be seen that the strain transients are shifted towards higher values for each increasing SOC, due to the strong dependence of the cell deformation on SOC discussed previously [8]. The comparison between the evolution of the temperature and the evolution of the strain shows that the latter can be used as an early safety alert throughout its dependence on SOC: the partially discharged cells are more “retracted” (i.e. the strain is negative, considering SOC = 100 % as a reference point with zero stain) and more resistant against thermal abuse and vice versa.

It should be also denoted that according to the product datasheet of the adhesive bonding material M-Bond 200 (Micro-Measurements, USA), it is possible to deliver reliable long-term stain measurements at temperatures up to 65°C and reliable short-term stain measurements at temperatures up to 95°C. Thus, the obtained data on the cell deformation during the ARC tests can

be considered “semi-quantitative” above the temperature limit of 65 °C and “qualitative” at T > 95°C (in contrast with the short-circuit tests are much more rapid). When the temperature exceeds 90 °C, the first cell starting to show irregularities in the strain behavior is the overcharged one. The observed anomaly is comprised in abrupt drop of the strain corresponding to a shrinking of the cell diameter. Similar drop is obtained at the other three cells, however the temperature corresponding to its appearance increases with the increase of the depth of discharge of the cells. It should be denoted that in the case of the cells with SOC equal to 0, 50 and 100, the temperature corresponding to this abrupt deformation (it is noted in Fig. 7f) is markedly higher than the temperature of the voltage drop indicated in Figure 7b. A closer inspection of the temperature transients (the inset in Fig. 7a) shows that there are small spikes coinciding very well with the moments of the abrupt deformation. In the case of the data corresponding to the cell with SOC = 100 %, the spike corresponds to a local temperature maximum of 120.5 °C which is fairly close to the endothermal phenomenon at 118 °C detected during the initial ARC test (Fig. 6). The only phenomenon able to explain such behavior of the observed cell parameters is the opening of the cell valve due to the increasing gas pressure inside. The valve opening and the corresponding pressure release cause instantaneous shrinkage of the cell similar to those observed in Figure 5. In the same time, vapors of the electrolyte solvent start leaving the cell causing the appearance of the endothermic heat effect. The venting point shifts gradually towards higher temperatures with the increase of the depth of discharge. Since the electrolyte concentration in the Li-ion cell does not depend on SOC, it is clear that the pressure build up does not correspond to a boiling process, but to chemical reactions such as the decomposition of SEI or the solvent oxidation at the positive electrode.

Further comparison of the data shown in Figure 7d-7e with those presented in Figure 5 shows a great difference in the strain variation from the point of the CID activation and the safety valve opening. This result can be related to the adhesive polymer material creep due to the high temperature and the long duration of the ARC experiments.

Figure 7c presents the evolution of the strength of the received acoustic signal during the four thermal abuse tests. When this parameter is used for “first order” analysis of the thermal abuse process, it can be seen that the progressive increase of the temperature leads to a decrease of the signal strength indicating an increased absorption of ultrasound by the cell materials. Figure 8 presents the analysis of the ultrasound interrogation data using data mapping and clustering. Figure 8a shows that the signal strength decreases almost linearly with the temperature. The signal is lost for temperature higher than 92 °C for the cell at SoC 0 %, 130°C for the cells at SoC 50 % and 100 % or 145 °C for the overcharge cell. These thresholds exceed markedly the temperature limits specified in the product datasheet of the of the transducers EPZ-20MS64W (maximum operating temperature of 70°C and maximum storage temperature equal to 80°C). The data-mapping of the power spectral density presented in Figure 8b-8d indicates that the ultrasound interrogation method is able to distinguish the transition of the cell temperature from its normal operation domain (T ~ 35 – 60°C) to the domain of the overheating, where temperature exceeds the onset point of 60°C. These temperatures are well below the above-mentioned transducer operation limits, which means that such indication can be used as early battery safety alert. This hypothesis can be confirmed by the comparison of the power spectral density plots shown also in Figure 8b-8c for the cases of cells with “normal” SOC values. It can be seen that in all three cases the PSD comprise a main peak centered at 125kHz and a couple of peaks with power intensity at higher frequencies. The increase of the temperature above the onset point results in considerable decrease of the main peak and rather small change of the minor peaks at the higher frequencies. This particular result shows that the ultrasound interrogation and the corresponding signal mapping and clustering is a sensitive method for early detection of slowly approaching thermal abuse events.

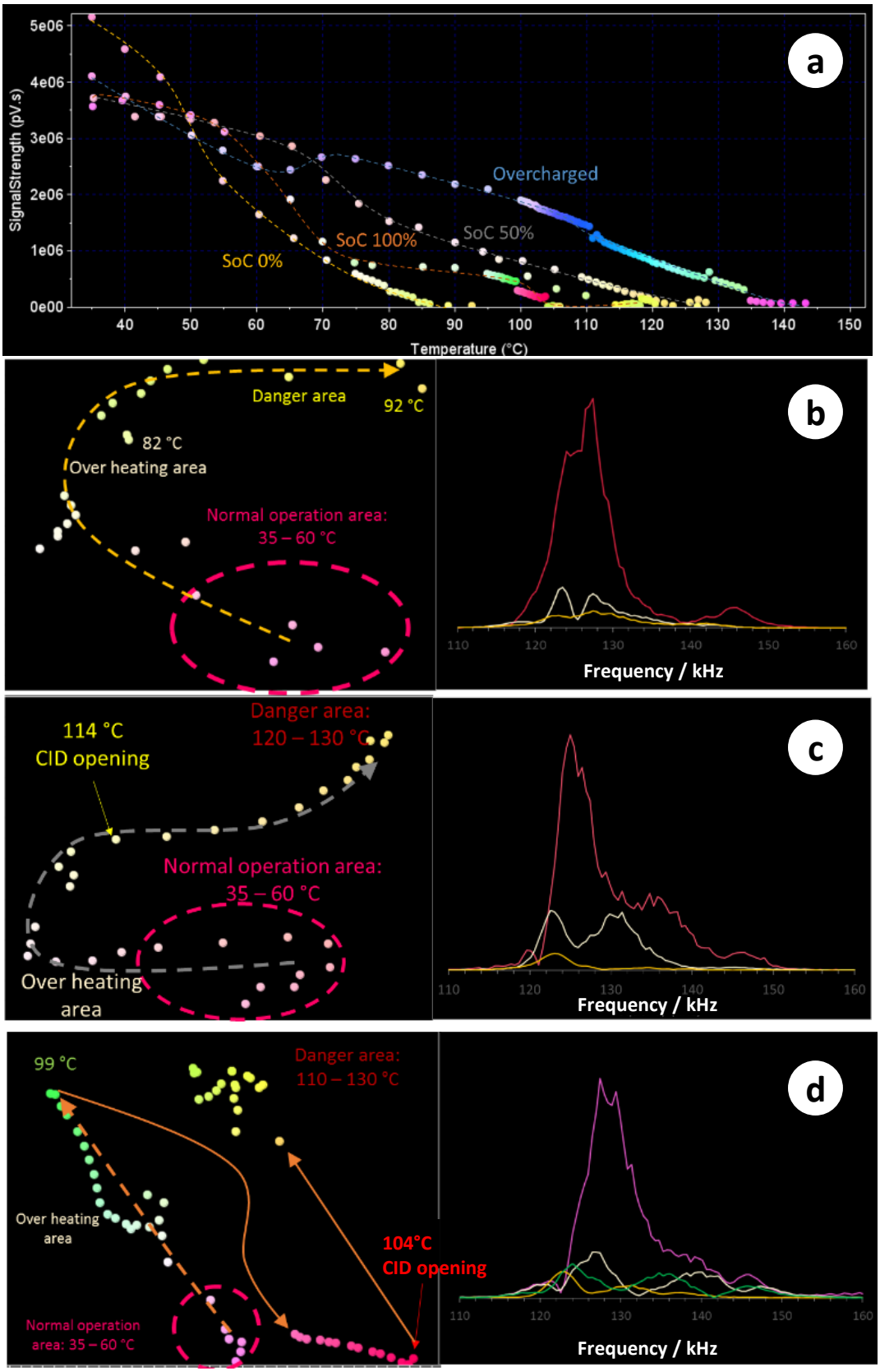

Fig. 8. Signal strength evolution (a) and clustering and mapping of the accosting ultrasound interrogation signals measured during the thermal abuse tests of MJ1 cells at state of charge equal to 0% (b), 50% (c) and 100% (d).

4. Conclusions

Acoustic ultrasound interrogation and deformation measurements have been used simultaneously as supplementary battery monitoring methods during thermal safety tests of 18650 MJ1 NMC Li-ion cells. The experiments carried out in adiabatic rate calorimeter on completely charged and overcharged batteries, showed that the selected Li-ion technology is susceptible to self-heating by slow internal exothermic reactions starting above 60 °C. More violent thermal runaway process starts when the temperature approaches and exceeds 140 °C. In contrast, when the cells are at SOC = 50 % or less, they remain stable at temperature lower than 160°C. The results from the extended monitoring of the cells during the thermal stability tests showed that the acoustic ultrasound interrogation combined with a data mapping and clustering provides indication for approaching battery safety breach events. It has been seen that both the acoustic signal and the strain correlates well with the increase of the temperature. However, in both cases the correlation becomes qualitative above 80°C due to the technical limits of the selected strain gages and the piezoelectric transducers.

The external short-circuit safety tests showed that the MJ1 technology is protected against this type of thermal abuse by CID integrated in the positive terminal of the cell. The experiments employing mechanical battery monitoring has been applied for a wide range of conditions in terms of cell SOC and electric resistance of the short-circuit. It has been seen that the most intense cell heating can be produced when the SOC is close to 100 % and the short-circuit shunt resistance is between 20 and 40mOm. Lower values of the shunt resistance lead to faster heating and faster activation of the CID, while higher shunt resistance rates limit the discharge current. The mechanic monitoring results show that the strain gage is able to provide very rapid indication of this type of battery abuse due to the abrupt change of the cell pressure. It precedes the time of increase of the cell casing temperature by an order of magnitude.

Acknowledgement

This work has been realized in association with INES.2S within the French national program Investments for the Future (ANR-10-IEED-0014-01) and received funding from the European Union's Horizon 2020 research and innovation program under the grant 'Electric Vehicle Enhanced Range, Lifetime And Safety Through INGenious battery management' (Project EVERLASTING-713771).

References

1. F. Larsson and B.-E. Mellander, J Electrochem Soc 161 (2014) A1611

2. D. Juarez-Robles, S. Azam, J.A. Jeevarjan, and P.P. Mukherjee, J Electrochem Soc 168 (2021) 050535

3. H. Ji, Y.-H. Chung, X.-H. Pan, M. Hua, C.-M. Shu, L.-J. Zhang, J Thermal Analysis Calorimetry 144 (2021) 1065

4. R. Spotnitz J. Franklin, J Power Sources 113 (2003) 81

5. Thi Thu Dieu Nguyen, Sara Abada, Amandine Lecocq, Julien Bernard, Martin Petit,

Guy Marlair, Sylvie Grugeon, Stéphane Laruelle, World Electric Vehicle Journal 10 (2019) 79

6. Soroosh Sharifi-Asl, Jun Lu, Khalil Amine, Reza Shahbazian-Yassar, Adv. Energy Mater. 9 (2019) 1900551

7. X. Feng, M. Ouyang, X. Liu, L. Lu, Y. Xia, X. He, Energy Storage Materials 10 (2018) 246

8. A. Kirchev, N. Guillet, D. Brun-Buission, V. Gau, J Electrochem Soc 169 (2022) 010515

9. H. Maleki, S. Al Hallaj, J.R Selman, R.B. Dinwiddie, H. Wang, J Electrochem Soc 146 (1999) 947

10. Jean Avril, “Encyclopédie Vishay d'analyse des contraintes encyclopédie”, NT 58C “Interpretation des mesures extensometriques”, Micromesures, 1984

11. Weisi Li, K.R. Crompton, Christopher Hacker, Jason K. Ostanek, J Energy Storage 32 (2020) 101890